Turkish Journal of Neurology

Turk J Neurol 2024;30(3):173-184
Doi: 10.55697/tnd.2024.144

ORIGINAL ARTICLE

Analysis of white matter hyperintensities in Alzheimer's disease and vascular dementia with magnetic resonance imaging

Seval Torun Yeter[1], Serkan Tüzün[2], Fatoş Dağdelen[3], İbrahim Acır[3], Fırat Kaçar[2], Vildan Ayşe Yayla[3]

[1]Biomedical Engineering Program, İstanbul University - Cerrahpaşa, İstanbul, Türkiye
[2]Electrical - Electronics Engineering, İstanbul University - Cerrahpaşa, İstanbul, Türkiye
[3]Department of Neurology, Bakırköy Dr. Sadi Konuk Training and Research Hospital, İstanbul, Türkiye

ABSTRACT

Objectives: The study aimed to analyze the brain white matter hyperintensities (WMHs) of patients with vascular dementia (VaD) and Alzheimer's disease (AD) using magnetic resonance imaging to determine whether white matter lesions in the brain could be detected by a computer using image processing methods.

Patients and methods: In this retrospective observational study, a unimodal, unsupervised, and automatic method was developed, and magnetic resonance imaging of 35 patients were examined. Of the 35 patients, 19 (14 males, 5 females; mean age: 73.2±6.7 years; range, 56 to 83 years) were picked from patients with AD or VaD who were admitted to a neurology clinic between January 2016 and December 2022 (Group 1). The remaining 16 patients (10 females, 5 males; mean age: 80.4±5.4 years; range, 69 to 92 years) were included from the ABVIB (Aging Brain: Vasculature, Ischemia, and Behavior) study from the ADNI (Alzheimer's Disease Neuroimaging Initiative) database (Group 2). To calculate the volume of WMHs, a detailed analysis was conducted. Initially, skull stripping was performed, and then the brain was segmented. Afterward, two types of masks (Mask-1 and Mask-2) were obtained by applying painting, decreasing, and blurring processes to the segmented white matter. These masks limited the region that was searched for WMHs. With this limitation, false positives that could arise from gray matter intensities were tried to be prevented. To evaluate the accuracy of WMH detection, a user interface was developed, and manual marking was conducted by an expert neurologist. After WMH detection, WMH volumes were calculated.

Results: For Group 1, the similarity index was found to be 0.76 for Mask-1 and 0.80 for Mask-2, while for Group 2, the similarity index was 0.71 for Mask-1 and 0.87 for Mask-2. In patients with AD, the mean WMH lesion load (LL) was 15.16±16.59 mL. In patients with VaD, who were expected to suffer more from WMHs, the mean WMH LL was 29.22±11.40 mL. In Group 2, the mean WMH LL was 17.77±12.26 mL.

Conclusion: This study may contribute to the literature since it is an automatic, unimodal, and unsupervised method that was applied to both a completely unique data set with many different scanning parameters and an open database data set.

Keywords: Alzheimer's disease, magnetic resonance image, vascular dementia, white matter hyperintensity.

Patients who have experienced vascular health issues, such as stroke and hypertension, often have white matter hyperintensities (WMHs) in their brains.[1] White matter hyperintensities are areas of tissue that result from the demyelination of myelinated axons of neurons in the white matter (WM) of the brain.[2-4] While WMHs can also be observed in healthy individuals, they are generally considered to be indicators of certain neurological diseases that predominantly affect elderly people, such as vascular dementia (VaD), cognitive impairment, stroke, and cerebrovascular disease. White matter hyperintensities are also detected in individuals with VaD and in nearly 60% of patients

Correspondence: İbrahim Acır, MD. Bakırköy Dr. Sadi Konuk Eğitim ve Araştırma Hastanesi, Nöroloji Kliniği, 34147 Bakırköy, İstanbul, Türkiye.
E-mail: iacir33@gmail.com
Received: February 29, 2024 **Accepted:** August 05, 2024 **Published online:** September 06, 2024
Cite this article as: Torun Yeter S, Tüzün S, Dağdelen F, Acır İ, Kaçar F, Yayla VA. Analysis of white matter hyperintensities in Alzheimer's disease and vascular dementia with magnetic resonance imaging. Turk J Neurol 2024;30(3):173-184. doi: 10.55697/tnd.2024.144.

with Alzheimer's disease (AD).[5] In clinical practice, computed tomography and magnetic resonance imaging (MRI) are commonly used for detecting WMHs.

Many studies on WMHs are present in the literature.[2-10] It is possible to classify the methods for detecting WMHs in different ways (e.g., supervised/unsupervised, semi-automatic/fully automatic, and unimodal/multimodal). The advantages and disadvantages of these methods will be discussed in the discussion section. The most preferred method, unsupervised, unimodal, and fully automatic segmentation of WMH, is still not completely resolved. However, there are numerous studies on the quantitative segmentation of WMH in various patient groups.[2,3,6,8,10-28]

This study proposed an unsupervised, automated, and unimodal method for age-related WMH detection by studying both images from real patients with dementia and open database images. For this purpose, the brain was segmented, and then two types of masks (Mask-1 and Mask-2) were developed in Matrix Laboratory (MATLAB, version R2018b) by applying painting, decreasing, and blurring processes to the segmented WM. These masks were applied to images to limit the regions of interest (ROI) with WMHs. With this limitation, we aimed to prevent false positives (FPs) that may arise from gray matter (GM) intensities. An interface that allows manual marking of true and falsely detected areas was developed to evaluate the performance of detection.

PATIENTS AND METHODS

In this retrospective observational study, two types of data were used. First, axial T2-weighted FLAIR (fluid-attenuated inversion recovery) MRI scans of 19 patients who were admitted to the neurology clinic of the Bakırköy Dr. Sadi Konuk Training and Research Hospital between January 2016 and December 2022 were used (Group 1). The determination of images for the data set was pointed out by an expert neurologist. Since MRI scans were achieved with very different protocols for Group 1, the data acquisition protocols are presented in Table 1.

Beside this unique data set, we aimed to demonstrate the validity of this method on images taken according to a fixed protocol. Therefore, the Alzheimer's Disease Neuroimaging Initiative (ADNI) database, in which MRI and other scans and biosamples of neurological patients are available through different application processes,[29] was applied. Images and data from the ADNI database were used in different studies in the literature.[28,30,31] To be coherent with the subject of this study, data from subjects with vascular or ischemic disease were preferred. The ABVIB (Aging Brain: Vasculature, Ischemia, and Behavior) study provided the necessary data.[29] Sixteen axial T2-weighted FLAIR MRI scans from the ABVIB study were analyzed in this study (Group 2). According to the DICOM (Digital Imaging and Communications in Medicine) tags, these 16 images were scanned with a GE Signa HDxt device (General Electric Healthcare, Chicago, Illinois, USA), which has three Tesla magnetic fields. All images had 42 slices, with a slice thickness of 5 mm and pixel spacing of 0.8594\0.8594.

In Group 1, 15 patients had AD (10 males, 5 females; mean age: 74±5.3 years; range, 64 to 84 years). The remaining four patients had VaD (all male; mean age: 70.3±11.3 years; range, 59 to 82 years). The mean age of all 19 patients in Group 1 was 73.2±6.7. Group 2 included 16 patients with WMHs (10 females, 5 males; mean age: 80.4±5.4 years; range, 69 to 92 years). One patient in Group 2 did not declare their sex.

In this study, WMH determination was studied only using FLAIR images. The flowchart of the WMH detection method is shown in Figure 1.

Skull stripping

Skull stripping (brain extracting), which is usually the first step in brain image processing, is concerned with the separation of the predominant tissues of the brain (GM, WM, and cerebrospinal fluid) from other tissues. In this study, BET (Brain Extraction Tool), a tool of the FMRIB Software Library developed at Oxford University,[32] was used for skull stripping. After skull stripping, intensity values of each image were normalized to the range of 0 to 255.

Creating the WM Mask-1

White matter hyperintensities appear brighter than the surrounding healthy WM tissue; however, their intensities are quite similar to GM intensities in FLAIR modality, which makes WMH determination more challenging. In some studies, it was observed that various postprocessing steps were preferred to correct false positives, such as GMs classified as WMHs or the effects of flow artifacts.[2,3,6,10,14,20,22,23,25,26] In this study, it was assumed that excluding GMs from the ROI can prevent false positives at the beginning of the

TABLE 1
Magnetic resonance imaging protocols

Type ID	Age/Sex	Device	Magnetic field	Number of slices	Slice thickness	TR (ms)	TE (ms)	TI (ms)	Flip angel	Matrix size	Pixel size
AD 1	67/M	Siemens magnetom verio	3T	20	5 mm	9000	81	2500	150	320×240	0.71875×0.71875
AD 2	73/M	Siemens magnetom amira	1.5T	23	5 mm	9000	82	2500	150	512×384	0.48828125×0.48828125
AD 3	80/F	Siemens magnetom amira	1.5T	21	5 mm	9000	82	2500	150	512×384	0.48828125×0.48828125
AD 4	77/M	Siemens magnetom symphony	1.5T	21	5 mm	9300	113	2500	150	512×360	0.48828125×0.48828125
AD 5	77/M	Siemens magnetom amira	1.5T	21	5 mm	9000	82	2500	150	512×384	0.48828125×0.48828125
AD 6	82/M	Siemens magnetom amira	1.5T	21	5 mm	9000	82	2500	150	512×384	0.48828125×0.48828125
AD 7	68/F	Siemens magnetom amira	1.5T	22	5 mm	9000	82	2500	150	512×384	0.48828125×0.48828125
AD 8	78/F	Ge brivo	1.5T	24	5 mm	9000	64	2500	90	512×512	0.4883×0.4883
AD 9	75/M	Siemens magnetom amira	1.5T	23	5 mm	9000	82	2500	150	512×384	0.48828125×0.48828125
AD 10	81/M	Siemens magnetom avanto	1.5T	21	5 mm	428	9,7		90	320x256	0.71875×0.71875
AD 11	66/M	Siemens magnetom symphony	1.5T	21	5 mm	9300	113	2500	150	512×360	0.48828125×0.48828125
AD 12	67/F	Siemens magnetom avanto	1.5T	21	5 mm	10270	69	2500	150	640×416	0.40625×0.40625
AD 13	73/F	Siemens magnetom avanto	1.5T	22	5 mm	10000	66	2500	150	320×224	0.8125×0.8125
AD 14	73/M	Siemens magnetom amira	1.5T	21	5 mm	9000	82	2500	150	512×384	0.48828125×0.48828125
AD 15	73/M	Siemens magnetom verio	3T	20	5 mm	9000	81	2500	150	320×240	0.71875×0.71875
VaD 1	83/M	Siemens magnetom verio	3T	20	5 mm	9000	81	2500	150	320×240	0.71875×0.71875
VaD 2	68/M	Siemens magnetom aera	1.5T	22	5 mm	9000	82	2500	150	512×448	0.44921875×0.44921875
VaD 3	74/M	Siemens magnetom amira	1.5T	21	5 mm	9000	82	2500	150	512×384	0.48828125×0.48828125
VaD 4	56/M	Siemens magnetom amira	1.5T	21	5 mm	9000	82	2500	150	512×384	0.48828125×0.48828125

ID: Identifier; TR: Repetition time; TE: Echo time; TI: Inversion time; AD: Alzheimer's disease; VaD: Vascular dementia.

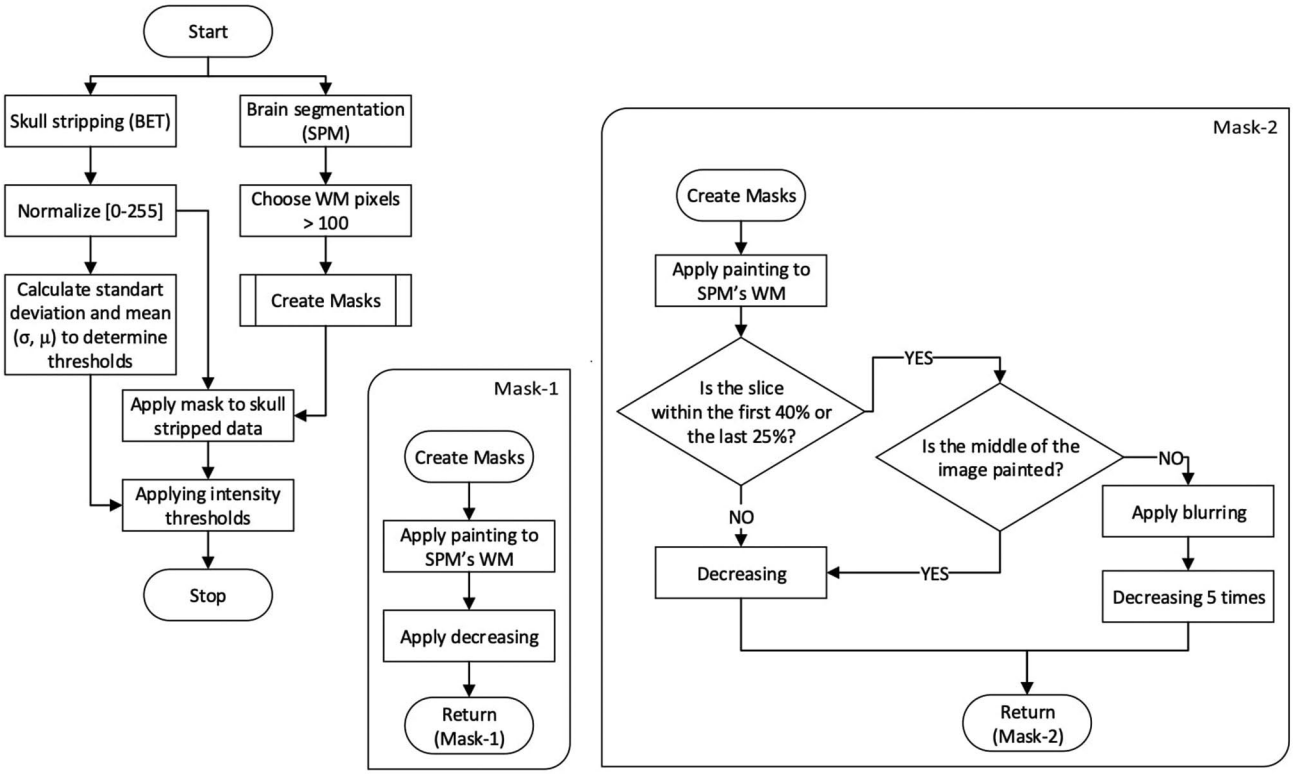

Figure 1. Flowchart of the WMH detection method.

WMH: White matter hyperintensity; BET: Brain extraction tool; SPM: Statistical parametric mapping; WM: White matter.

process. Thus, the aim was to determine WMHs only in WM areas. First, the brain was segmented to identify the WM. For WM segmentation, statistical parametric mapping (SPM, version SPM12), a MATLAB-based program developed by University College London, was used. Statistical parametric mapping has open-source code, and it allows users to develop new routines; therefore, it is frequently used in the literature.[3,33,34] In this study, segmentation was processed in native space. Sample distance was set to default,[3] affine regularization was applied using the ICBM template for European brains, smoothness was set to default (0), and the number of Gaussians was set to 1. White matter areas segmented by SPM were not used to determine WMHs but rather to determine the boundaries within which WMHs could be identified. The detection of WMH could be conducted on skull-stained images or usual images.

As mentioned before, WMHs contrast with WM but are similar to healthy GM intensities. Therefore, when we analyzed the areas determined by SPM as WM, some included WMH areas, while others did not. To overcome this challenge, a better mask was created to SPM's WM areas. To determine the outer boundaries of the WM segmented by SPM and to use the inner areas as a mask, an algorithm called "painting" was developed on MATLAB. In painting, the image was scanned with a 3×3 window, and a negative value was assigned to all pixels that were adjacent to the initial pixel. Thus, WMH areas, which were inside the WM but were not classified as WM by SPM remained nonnegative, unless they were adjacent to non-WM pixels. After painting, pixels of nonnegative values were assigned 1, and pixels of negative values were assigned as 0. Thus, a mask that consisted of only 1s and 0s was obtained.

In case the pixels close to GM features in the outer boundaries were observed, 1 pixel was decreased from the outer boundaries of the mask. This process was called "decreasing." After painting and decreasing, Mask-1 was obtained and applied. Figure 2 demonstrates an example of Mask-1.

Creating Mask-2 by Improving Mask-1

Painting presented expected results in images where SPM's WM boundaries drew a closed shape

Figure 2. An example for Mask-1. **(a)** Skull-stripped image, **(b)** Mask-1 and **(c)** applying Mask-1 to skull-stripped image.

around the ventricles (Figure 2). However, in images where ventricles were neighbored by areas outside the brain tissue, some WMHs were not included in the mask (Figure 3). Therefore, Mask-1 needed improvement.

The Mask-2 algorithm checked whether there was a negative value in the middle of the image after painting. If there was one, the image was blurred by a Gaussian filter before painting. This was called "blurring." With blurring, it was aimed to close the little gaps that caused the painting process to involve the ventricles and to include the WMHs that were near the ventricles, which were included in the mask (Figure 4). However, besides these WMH pixels, blurring could cause unnecessary pixels at the boundaries. For this reason, decreasing was applied to blurred images five times (the number was determined empirically). After all these steps, Mask-2 was obtained. Images obtained with these processes are shown in Figure 4. As shown in Figure 4, Mask-2 included areas that could not be included by Mask-1 in Figure 3.

The intensity threshold

This step aimed to determine the pixels whose intensities were above the threshold as WMHs by applying an intensity threshold to the masked images. Mean and standard deviation values were used to determine the threshold value, as in some other studies.[21-23]

The mean and standard deviation values of the data were calculated. The threshold values were empirically calculated according to Equation 2.1, as shown below:

$$th = \begin{cases} \mu+20\sigma & \text{if } \sigma \le 5 \\ \mu+10\sigma & \text{if } 5 < \sigma \le 9 \\ \mu+2\sigma & \text{if } 9 < \sigma \le 15 \\ \mu+1{,}25\sigma & \text{if } 15 < \sigma \le 40 \\ \mu+\sigma & \text{o.w.} \end{cases} \quad (2.1)$$

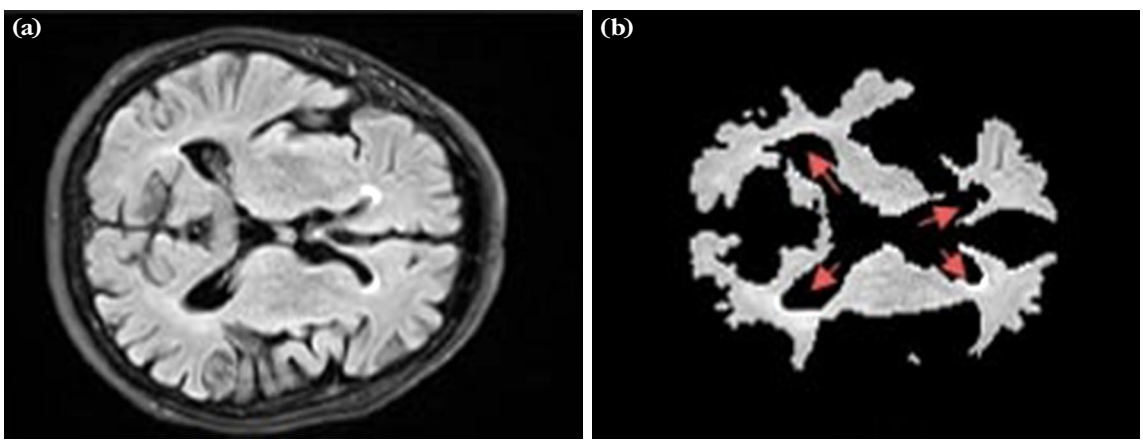

Figure 3. White matter hyperintensities were not included in the mask shown with red arrows. **(a)** Original images, **(b)** applying Mask-1.

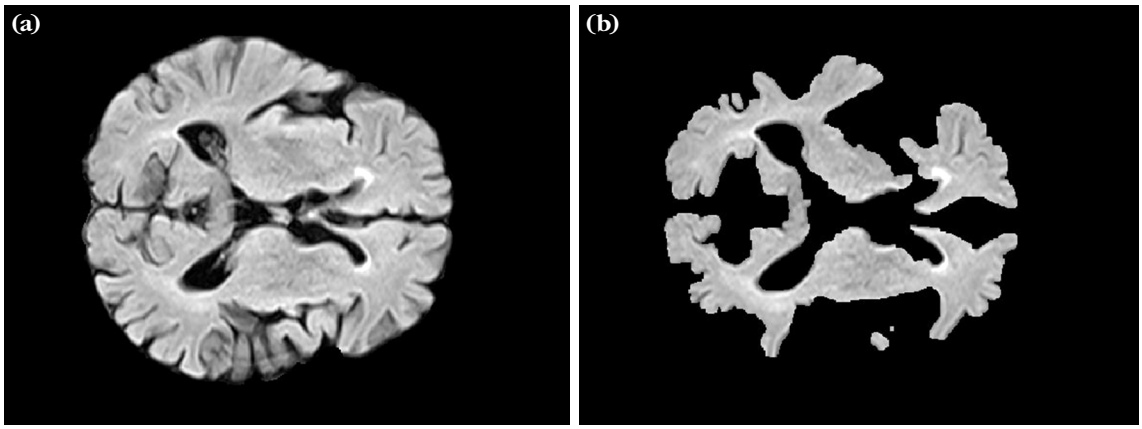

Figure 4. An example for Mask-2. **(a)** Skull stripped image, **(b)** Applying Mask-2.

After the intensity threshold was applied, determined WMHs smaller than 5 pixels were removed (the number was determined empirically) for FP reduction. The estimated WMHs after these steps are shown in Figure 5.

Lesion load (LL) calculation

White matter hyperintensity volumes were calculated using the data presented in Table 1. The volume of a voxel (V) was calculated with the following formula:

$$V = st \times ps^2 \quad (2.2)$$

Here, st represented slice thickness, and ps represented pixel size. Afterward, the total number of voxels was multiplied by the volume of a voxel. The final volumes are presented in Tables 2 and 3 for Group 1 and Table 4 for Group 2.

Evaluation

In many studies, the results of WMH detection were evaluated by comparing them with the manual segmentation performed by an expert neuroradiologist.[2,3,6,10-12,14-17,19-22,24-27] Similarly, manual marking performed by a specialist neurologist was used for evaluation in this study. A user interface was developed with MATLAB App Designer, and true positive (TP), FP, false negative (FN), and true negative (TN) areas were determined. After obtaining TP, FP, and FN, the images were colorized as shown in Figure 6 for Group 1 and Group 2.

After these steps, the similarity index (SI) and sensitivity values were calculated to measure the performance of the proposed method.[8,16,24]

$$SI = \frac{2TP}{2\ TP+FP+FN} \quad (2.3)$$

$$Sensitivity = \frac{TP}{TP+FN} \quad (2.4)$$

The codes used in this study are available on GitHub.[35]

Figure 5. Estimated WMHs. **(a)** Skull-stripped image, **(b)** estimated WMHs using Mask-1, and **(c)** estimated WMHs using Mask-2.

WMHs: White matter hyperintensities.

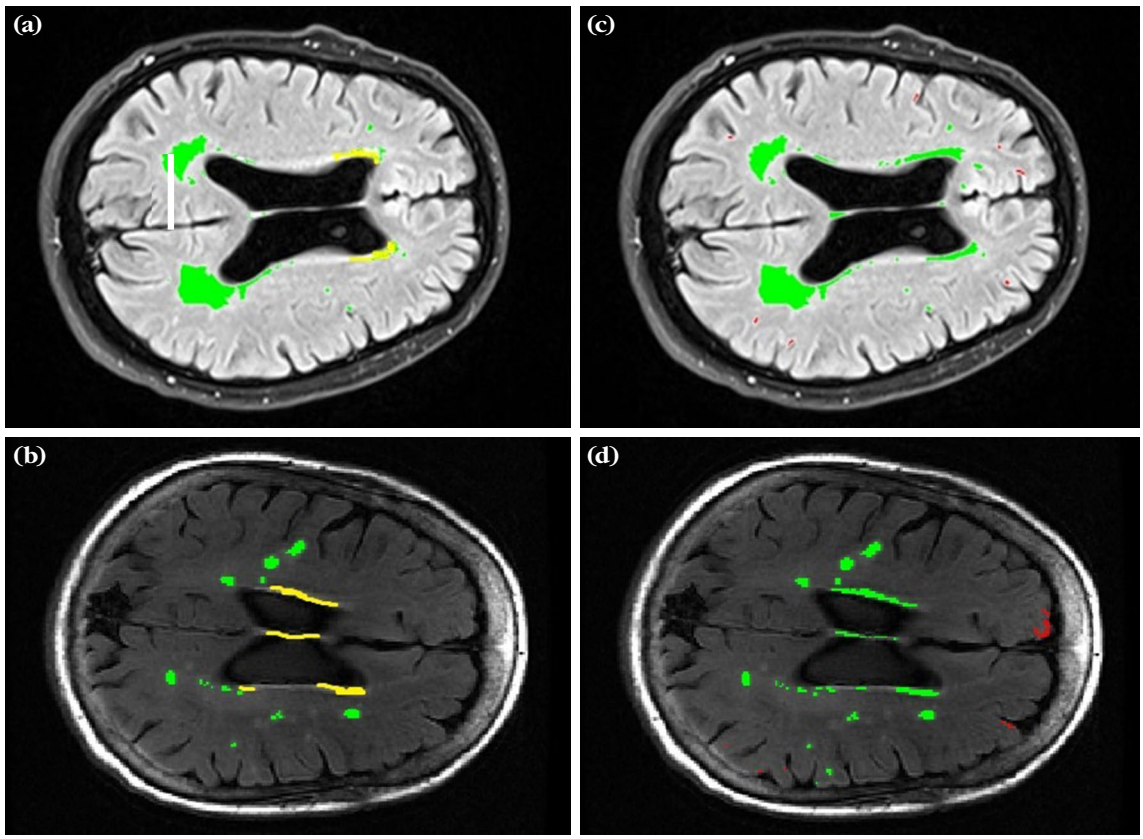

Figure 6. Evaluation of automatic segmentation with manual segmentation. The images were colorized after obtaining TP (green), FP (red), and FN (yellow). **(a, b)** Mask-1, **(c, d)** Mask-2.

TP: True positive; FP: False positives FN: False negative.

RESULTS

Brain WMH volumes were analyzed in both AD and VaD patients and the MRI scan protocols used for these analyses are detailed in Table 1.

When Table 2 is analyzed, the mean WMH LL for AD was 15.16±16.59 mL. For VaD, the mean WMH LL was 29.22±11.40 mL, approximately twice the LL in AD.

As for Group 2, since the patients' clinical findings could not be retrieved, the type of disease they had could not be determined. The mean WMH LL was calculated as 17.77±12.26 mL for Group 2.

Tables 3 and 4 present the SI and sensitivity values for both Mask-1 and Mask-2 across different LL categories.

TABLE 2
Calculated WMH LL values

	AD														
Type ID	1	2	3	4	5	6	7	8	9	10	11	12	13	14	15
LL (mL)	0.42	17.87	21.14	2.18	5.27	59.74	18.04	1.50	38.68	3.65	7.23	4.52	14.63	4.42	28.13
Average (mL)	15.16±16.59														
	VaD														
Type ID	1	2	3	4											
LL (mL)	40.27	13.37	33.26	29.97											
Average (mL)	29.22±11.40														

WMHs: White matter hyperintensities; LL: Lesion load: ID: Identifier; AD: Alzheimer's disease; VaD: Vascular dementia.

TABLE 3
Similarity indices and sensitivity values

Type ID	LL (mL)	Mask-1 SI	Mask-1 sensitivity	Mask-1 (Average SI)	Mask-2 SI	Mask-2 sensitivity	Mask-2 (Average SI)
AD 6	59.74	0.99	0.97		0.98	0.95	
VaD 1	40.27	0.98	0.98	High LL	0.98	0.99	High LL
AD 9	38.68	0.98	0.96		0.97	0.96	
VaD 3	33.26	0.99	0.99		0.98	0.99	
VaD 4	29.97	0.98	0.97		0.99	0.98	
AD 15	28.13	0.99	0.97		0.98	0.97	
AD 3	21.14	0.77	0.79		0.87	0.99	
AD 7	18.04	0.97	0.96	Medium LL	0.98	0.98	Medium LL
AD 2	17.87	0.82	0.92		0.85	0.97	
AD 13	14.63	0.89	0.94		0.87	0.93	
VaD 2	13.37	0.68	0.53		0.95	0.95	
AD 11	7.23	0.73	0.64		0.84	0.94	
AD 5	5.27	0.66	0.81		0.57	0.94	
AD 12	4.52	0.90	0.92		0.89	0.96	
AD 14	4.42	0.20	0.11	Low LL	0.78	0.66	Low LL
AD 10	3.65	0.18	0.10		0.44	0.40	
AD 4	2.18	0.66	0.56		0.61	0.80	
AD 8	1.5	0.37	0.48		0.38	0.85	
AD 1	0.42	0.71	1.00		0.28	1	
Averages		0.76	0.77		0.80	0.91	

ID: Identifier; LL: Lesion load: SI: Similarity index; AD: Alzheimer's disease; VaD: Vascular dementia.

TABLE 4
Lesion load, SIs, and sensitivity values for ABVIB images

Type ID	LL (mL)	Mask-1 SI	Mask-1 sensitivity	Mask-1 (Average SI)	Mask-2 SI	Mask-2 sensitivity	Mask-2 (Average SI)
PwWM 1	49.48	0.99	0.99		0.99	0.99	
PwWM 2	31.48	0.73	0.60	High LL	0.94	0.94	High LL
PwWM 3	30.67	0.99	0.99		0.99	1.00	
PwWM 4	24.56	0.99	0.98		0.99	0.98	
PwWM 5	22.30	0.86	0.76		0.99	1.00	
PwWM 6	20.06	0.88	0.82		0.99	1.00	
PwWM 7	19.36	0.98	0.96	Medium LL	0.99	0.99	Medium LL
PwWM 8	18.52	0.08	0.04		0.50	0.35	
PwWM 9	15.33	0.69	0.84		0.82	0.91	
PwWM 10	14.09	0.97	0.95		0.99	0.99	
PwWM 11	10.12	1.00	1.00		1.00	1.00	
PwWM 12	7.62	0.26	0.15		0.97	0.94	
PwWM 13	7.01	1.00	1.00		1.00	1.00	
PwWM 14	5.58	0.73	0.84	Low LL	0.83	0.99	Low LL
PwWM 15	4.31	0.06	0.03		0.08	0.04	
PwWM 16	3.91	0.10	0.06		0.80	0.67	
Averages	17.78	0.71	0.69		0.87	0.86	

ID: Identifier; SI: Similarity index; ABVIB: Aging Brain: Vasculature, Ischemia, and Behavior; LL: Lesion load.

In Group 1, the mean SI was 0.76 for Mask-1 and 0.80 for Mask-2. Lower SI values were reached in both masks at low LL (Mask-1 mean: 0.55; Mask-2 mean: 0.60). However, these values were enhanced in medium and high LL. The mean SI was calculated as 0.87 for Mask-1 and 0.93 for Mask-2 in medium LL (10 mL< LL ≤30 mL), whereas it was 0.99 for Mask-1 and 0.97 for Mask-2 in high LL (>30 mL).

In Group 2, the mean SI was 0.71 for Mask-1, and the algorithm was more successful for Group 1 in Mask-1. The mean SI was 0.87 for Mask-2, which shows that the algorithm was more successful for Group 2 in Mask-2. On the other hand, when we analyzed the evaluation values in Tables 3 and 4, the ratios were consistent between Group 1 and Group 2.

DISCUSSION

In this study, brain WMHs of patients with dementia were analyzed via MRI using a unimodal, automatic, and unsupervised method. As mentioned in the introduction section, there are different methods for WMH segmentation: unimodal/multimodal, automatic/manual, and supervised/unsupervised. This study primarily aimed to detect WMHs correctly via a unimodal, fully automatic, and unsupervised method.

The reasons for using a unimodal, fully automatic, and unsupervised method in the study are numerous. First, unimodal studies have more advantages than multimodal studies. Multimodal studies need more than one MRI modality,[11,12,20] and this causes some disadvantages. The acquisition of several volumes for each patient is expensive and requires a registration algorithm, which can introduce errors and increase complexity.[24] Moreover, the patients stay in the MRI scanner for a longer time, and this could cause motion artifacts.[24] As the number of images increases, memory requirements and the computational complexity of the algorithm increase.[10,24] For these reasons, a unimodal method was developed in this study. When developing this unimodal method, the FLAIR modality was preferred since WMHs are detected best in FLAIR images. However, there are hyperintense artifacts that may cause FPs in FLAIR images. To utilize the FLAIR modality, masking processes were developed to prevent FPs; thus, we could use only the FLAIR modality to detect WMHs.

The most important advantage of automatic methods is that they do not need manual interference. Although there is no gold standard for WMH segmentation, except manual segmentation,[2,8,11-19] manual segmentation of the brain is time-consuming and labor-intensive. An experienced neuroradiologist requires significant time and effort to achieve results while studying images slice by slice. Moreover, these results suffer from high intraobserver and interobserver variability,[20] are fully prone to human errors, and are hardly practical, particularly in large-scale studies and longitudinal studies.[20] Semi-automatic methods are less time-consuming and more reproducible but still need user interaction;[36,37] therefore, they suffer from intraobserver and interobserver variability. Furthermore, they remain labor-intensive, particularly for large-scale studies.[12] For these reasons, we tried to use an automatic method for this study.

Supervised methods require manually segmented data for training.[28] The constraints of manual segmentation were previously mentioned. Therefore, we aimed for this study to be unsupervised.

Overall, it is apparent that unsupervised, fully automated, and unimodal methods are considered more advantageous and are often preferred.[16,21,24,28]

White matter hyperintensities are patchy, small, diffuse, irregular, faint, and vague; they can be nodular or confluent. Moreover, their locations are variable. They do not have a particular form, have fuzzy borders, and are inhomogeneous. Their intensities are quite similar to healthy GM. All these characteristics are among the factors that make WMH detection more challenging.

When determining WMHs, Mask-1 and Mask-2 were applied to the images aiming to limit the ROI. Mask-1 and Mask-2 were obtained by applying modifications to WM regions segmented by SPM. Segmentation algorithms in SPM might be sensitive to the presence of large abnormalities in the brain. Therefore, the possibility of the WMH segmentation being affected by the SPM process was eliminated in this study since the WMH determination was conducted in the skull-stained images and not in SPM images.

It is clear from Figures 6 that the blurring process caused a limited increase in FPs. Increasing FPs can be viewed as a disadvantage. However, when the total result was evaluated according to the SI value, Mask-2 was more successful than Mask-1 in both groups. This is because although FPs increase, FNs are remarkably decreased due to Mask-2. As can be observed in equation (2.4),

sensitivity was not affected by FP but only by TP and FN. Thus, reductions in FN in Mask-2 had more success on sensitivity values in both groups than SI (Figures 3, 4).

In WMH detection studies, SI values above 0.70 are considered to represent a good agreement between different segmentation methods.[10,26,38,39] Nevertheless, 0.70 can generally be achieved in data with medium and high LL. It is observed that success is generally reduced in low LL.[10,11,17,25,27] When the LL is lower, the effects of errors caused by segmentation or other reasons on the results increase.[10] Furthermore, in this study, a lower SI value was reached at low LL (Group 1, Mask-1 0.55 and Mask-2 0.60; Group2, Mask-1 0.43). Nevertheless, in Group 2, even in low LL, Mask-2 SI value was higher than 0.70 with 0.73. In medium and high LL, results were increasingly above 0.70, as shown in Tables 3 and 4.

Since WMH is the most prominent characteristic in VaD, these patients are expected to suffer from WMH more than patients with AD. Thus, in patients with VaD, WMH LL is expected to be higher, and the standard deviation is expected to be lower. White matter hyperintensity is not a prominent feature in AD; some patients with AD may exhibit it, while others may not. Therefore, in patients with AD, WMH LL is expected to be lower, and the standard deviation is expected to be higher. As mentioned before, WMH detection success is expected to increase with higher LL, and patients with VaD had a higher WMH LL than patients with AD in this study. Therefore, when we analyzed SI and sensitivity averages in each patient group, we saw that in patients with VaD, both algorithms had higher success.

As could be observed in Table 3 for Group 1, Mask-2 had higher SI and sensitivity averages than Mask-1, except for high LL. As mentioned before, the blurring process used in Mask-2 considerably reduced FNs but slightly increased FPs. False negatives were more common in medium and low LL. Thus, in data that had medium and low LL, even if FPs slightly increased, the reduction in FNs affected the results positively. In data that had high LL, FNs were uncommon, and SI was high (0.99). Therefore, even if there was a slight increase in FPs, SI was affected negatively by high LL. On the other hand, Table 4 for Group 2 shows that Mask-2 had higher SI and sensitivity values for all LL; therefore, it can be said that the reduction in FNs achieved a better result in Group 2.

According to the studies conducted in the literature,[1-28] it was observed that even if clinical data were used, MRI data were obtained with a particular protocol. Since this study was retrospective, MRIs were scanned by various technicians on different dates with different devices and using many different protocols (data acquisition protocols are given in Table 1). Although these differences increase the complexity of this study, this makes it more likely to adapt the study to be more similar to routine practice. However, to evaluate the validity of the method on images taken according to a fixed protocol, we also applied our method to ABVIB images and determined that in most criteria, our method showed consistent results between both groups. For example, as mentioned before, success increased with LL in both groups. Mask-2 demonstrated better success in both groups, as intended.

One of the strengths of this study was the use of a unimodal, fully automatic, and unsupervised method for detecting WMHs. The adoption of a unimodal approach reduces costs and complexity by eliminating the need for multiple MRI modalities. Using FLAIR images is highlighted as the most effective modality for detecting WMHs. The study developed specific masking processes to prevent false positives that could arise from FLAIR images. Automatic methods provide more efficient and reproducible results as they do not require manual intervention, which is especially important for large-scale and longitudinal studies. Additionally, they minimize human errors by reducing interobserver and intraobserver variability. The unsupervised approach allows data processing without the need for manual segmentation, eliminating the dependency on experienced neuroradiologists. Another significant strength of the study was its ability to be applied to retrospective MRI data scanned with various protocols. This adaptability makes the method more compatible with routine clinical practice. The application of Mask-1 and Mask-2 improved sensitivity and specificity indexes by significantly reducing FNs. Mask-2 demonstrated higher success rates due to its ability to reduce FNs.

The most important limitation of this study was the limited sample size. Only 19 patients' images were examined, with only four of them with VaD. Future studies should improve the methods and increase the number of samples, particularly for VaD. Additionally, applying different published methods to original data (Group 1) and comparing

them would be advantageous. A common shortcoming of WMH detection studies is lower accuracy in low LL.[9,15,16,24,26] A lower SI is often reached in low LL.[1,9,25] Similarly, in this study, lower SI values were achieved for both masks in Group 1 at low LL. However, in Group 2, even if Mask-1 showed restricted performance, Mask-2 could achieve SI values over 0.70 in every LL, including low LL. To further improve these results and achieve higher success, Mask-2 may be enhanced to reduce FPs, or different masks may be developed in future studies.

In conclusion, this study contributes to the literature by presenting an automatic, unimodal, and unsupervised method. It offers a unique dataset with diverse scanning parameters and is applied to images obtained following a standardized protocol. As the elderly population grows, age-related diseases such as dementia increase. Automatic, quantitative methods are essential for monitoring these diseases and analyzing WMHs.

Ethics Committee Approval: The study protocol was approved by the Bakırköy Dr. Sadi Konuk Training and Research Hospital, Clinical Research Ethics Committee (date: 26.03.2018, no: 2018-06-10). The study was conducted in accordance with the principles of the Declaration of Helsinki.

Patient Consent for Publication: A written informed consent was obtained from each patient.

Data Sharing Statement: The data that support the findings of this study are available from the corresponding author upon reasonable request.

Author Contributions: Idea, concept, writing, materials: S.T.Y.; Analyze, critical review: S.T.; Data collection, processing: F.D.; Draft, writing, analyze: İ.A.; Literature review: F.K.; Supervision: V.A.Y.

Conflict of Interest: The authors declared no conflicts of interest with respect to the authorship and/or publication of this article.

Funding: The authors received no financial support for the research and/or authorship of this article.

REFERENCES

1. Avcı AY, Toprak MK, Lakadamyalı H, Akıncı S. Mitral kapak prolapsusu, migren ve manyetik rezonans görüntülemede beyaz cevher hiperintensiteleri arasındaki ilişki. Turk J Neurol 2018;24:323-329 doi: 10.4274/tnd.04468
2. Gibson E, Gao F, Black SE, Lobaugh NJ. Automatic segmentation of white matter hyperintensities in the elderly using FLAIR images at 3T. J Magn Reson Imaging 2010;31:1311-22. doi: 10.1002/jmri.22004.
3. Maldjian JA, Whitlow CT, Saha BN, Kota G, Vandergriff C, Davenport EM, et al. Automated white matter total lesion volume segmentation in diabetes. AJNR Am J Neuroradiol 2013;34:2265-70. doi: 10.3174/ajnr.A3590.
4. Ghafoorian M, Karssemeijer N, Heskes T, van Uden IWM, Sanchez CI, Litjens G, et al. Location sensitive deep convolutional neural networks for segmentation of white matter hyperintensities. Sci Rep 2017;7:5110. doi: 10.1038/s41598-017-05300-5.
5. Fazekas F, Chawluk JB, Alavi A, Hurtig HI, Zimmerman RA. MR signal abnormalities at 1.5 T in Alzheimer's dementia and normal aging. AJR Am J Roentgenol 1987;149:351-6. doi: 10.2214/ajr.149.2.351.
6. Zhan T, Zhan Y, Liu Z, Xiao L, Wei Z. Automatic method for white matter lesion segmentation based on T1-fluid-attenuated inversion recovery images. IET Comput Vis 2015;4:447-455. doi: 10.1049/iet-cvi.2014.0121
7. Filippi M, Yousry T, Baratti C, Horsfield MA, Mammi S, Becker C, et al. Quantitative assessment of MRI lesion load in multiple sclerosis. A comparison of conventional spin-echo with fast fluid-attenuated inversion recovery. Brain 1996;119:1349-55. doi: 10.1093/brain/119.4.1349.
8. Qin C, Guerrero R, Bowles C, Chen, L, Dickie DA, Valdes-Hernandez MDC, et al. A large margin algorithm for automated segmentation of white matter hyperintensity. Pattern Recognition 2018;77:150-159. doi: 10.1016/j.patcog.2017.12.016
9. Scheltens P, Erkinjunti T, Leys D, Wahlund LO, Inzitari D, del Ser T, et al. White matter changes on CT and MRI: An overview of visual rating scales. European task force on age-related white matter changes. Eur Neurol 1998;39:80-9. doi: 10.1159/000007921.
10. Simões R, Mönninghoff C, Dlugaj M, Weimar C, Wanke I, van Cappellen van et al. Automatic segmentation of cerebral white matter hyperintensities using only 3D FLAIR images. Magn Reson Imaging 2013;31:1182-9. doi: 10.1016/j.mri.2012.12.004.
11. Anbeek P, Vincken KL, van Osch MJ, Bisschops RH, van der Grond J. Automatic segmentation of different-sized white matter lesions by voxel probability estimation. Med Image Anal 2004;8:205-15. doi: 10.1016/j.media.2004.06.019.
12. Admiraal-Behloul F, van den Heuvel DM, Olofsen H, van Osch MJ, van der Grond J, van Buchem MA, et al. Fully automatic segmentation of white matter hyperintensities in MR images of the elderly. Neuroimage 2005;28:607-17. doi: 10.1016/j.neuroimage.2005.06.061.
13. Wu M, Rosano C, Butters M, Whyte E, Nable M, Crooks R, et al. A fully automated method for quantifying and localizing white matter hyperintensities on MR images. Psychiatry Res 2006;148:133-42. doi: 10.1016/j.pscychresns.2006.09.003.
14. Zhiqiang Lao, Dinggang Shen, Jawad A, Karacali B, Dengfeng Liu, Melhem ER, et al. Automated Segmentation of White Matter Lesions in 3D Brain MR Images, using Multivariate Pattern Classification. In: 3rd IEEE International Symposium on Biomedical Imaging: Macro to Nano, 2006. Arlington, Virginia, USA: IEEE; 2006. p. 307-10.

15. Jeon S, Yoon U, Park J-S, Seo SW, Kim J-H, Kim ST, et al. Fully automated pipeline for quantification and localization of white matter hyperintensity in brain magnetic resonance image. Int J Imaging Syst Technol 2011;21:193-200.
16. Yoo BI, Lee JJ, Han JW, Oh SY, Lee EY, MacFall JR, et al. Application of variable threshold intensity to segmentation for white matter hyperintensities in fluid attenuated inversion recovery magnetic resonance images. Neuroradiology 2014;56:265-81. doi: 10.1007/s00234-014-1322-6.
17. Sudre CH, Cardoso MJ, Bouvy WH, Biessels GJ, Barnes J, Ourselin S. Bayesian model selection for pathological neuroimaging data applied to white matter lesion segmentation. IEEE Trans Med Imaging 2015;34:2079-102. doi: 10.1109/TMI.2015.2419072.
18. Griffanti L, Zamboni G, Khan A, Li L, Bonifacio G, Sundaresan V, et al. BIANCA (Brain Intensity AbNormality Classification Algorithm): A new tool for automated segmentation of white matter hyperintensities. Neuroimage 2016;141:191-205. doi: 10.1016/j.neuroimage.2016.07.018.
19. Park BY, Lee MJ, Lee SH, Cha J, Chung CS, Kim ST, et al. DEWS (DEep White matter hyperintensity Segmentation framework): A fully automated pipeline for detecting small deep white matter hyperintensities in migraineurs. Neuroimage Clin 2018;18:638-47. doi: 10.1016/j.nicl.2018.02.033.
20. Zijdenbos AP, Dawant BM, Margolin RA, Palmer AC. Morphometric analysis of white matter lesions in MR images: Method and validation. IEEE Trans Med Imaging 1994;13:716-24. doi: 10.1109/42.363096.
21. Keceli AS, Can AB, Automatic segmentation of white matter lesions. 2009 IEEE 17th Signal Processing and Communications Applications Conference, Antalya, Türkiye; 2009. p. 181-184, doi: 10.1109/SIU.2009.5136362.
22. de Boer R, van der Lijn F, Vrooman HA, Vernooij MW, Ikram MA, Breteler MMB, et al. Automatic segmentation of brain tissue andwhitematter lesions in MRI. In: 2007 4th IEEE International Symposium on Biomedical Imaging: From Nano to Macro . Arlington, VA: IEEE; 2007. p. 652-5.
23. Kruggel F, Paul JS, Gertz HJ. Texture-based segmentation of diffuse lesions of the brain's white matter. Neuroimage 2008;39:987-96. doi: 10.1016/j.neuroimage.2007.09.058. .
24. Khademi A, Venetsanopoulos A, Moody AR. Robust white matter lesion segmentation in FLAIR MRI. IEEE Trans Biomed Eng 2012;59:860-71. doi: 10.1109/TBME.2011.2181167.
25. Roy PK, Bhuiyan A, Janke A, Desmond PM, Wong TY, Storey E, et al. Automated Segmentation of White Matter Lesions Using Global Neighbourhood Given Contrast Feature-Based Random Forest and Markov Random Field. In: 2014 IEEE International Conference on Healthcare Informatics. Verona, Italy: IEEE; 2014. p. 1-6.
26. Wang R, Li C, Wang J, Wei X, Li Y, Hui C, et al. Automatic segmentation of white matter lesions on magnetic resonance images of the brain by using an outlier detection strategy. Magn Reson Imaging 2014;32:1321-9. doi: 10.1016/j.mri.2014.08.010.
27. Manjón JV, Coupé P, Raniga P, Xia Y, Fripp J, Salvado O. HIST: HyperIntensity Segmentation Tool. In: Wu G, Coupé P, Zhan Y, Munsell BC, Rueckert D, editors. Patch-Based Techniques in Medical Imaging. Cham: Springer International Publishing; 2016. p. 92-9.
28. Rachmadi MF, Valdes-Hernandez M del C, Komura T. Voxel-based irregularity age map (IAM) for brain's white matter hyperintensities in MRI. In: 2017 International Conference on Advanced Computer Science and Information Systems (ICACSIS) . Bali: IEEE; 2017. p. 321-6.
29. Alzheimer's Disease Neuroimaging Initiative (ADNI). Available at: https://adni.loni.usc.edu/ [Accessed: 22.04.2024]
30. Dadar M, Maranzano J, Misquitta K, Anor CJ, Fonov VS, Tartaglia MC, et al; Alzheimer's Disease Neuroimaging Initiative. Performance comparison of 10 different classification techniques in segmenting white matter hyperintensities in aging. Neuroimage 2017;157:233-49. doi: 10.1016/j.neuroimage.2017.06.009.
31. Bron EE, Smits M, van der Flier WM, Vrenken H, Barkhof F, Scheltens P, et al; Alzheimer's Disease Neuroimaging Initiative. Standardized evaluation of algorithms for computer-aided diagnosis of dementia based on structural MRI: The CADDementia challenge. Neuroimage 2015;111:562-79. doi: 10.1016/j.neuroimage.2015.01.048.
32. Smith SM. Fast robust automated brain extraction. Hum Brain Mapp 2002;17:143-55. doi: 10.1002/hbm.10062.
33. Withey DJ, Koles ZJ. Medical Image Segmentation: Methods and Software. In: 2007 Joint Meeting of the 6th International Symposium on Noninvasive Functional Source Imaging of the Brain and Heart and the International Conference on Functional Biomedical Imaging. Hangzhou, China: IEEE; 2007. p. 140-3.
34. García-Lorenzo D, Francis S, Narayanan S, Arnold DL, Collins DL. Review of automatic segmentation methods of multiple sclerosis white matter lesions on conventional magnetic resonance imaging. Med Image Anal 2013;17:1-18. doi: 10.1016/j.media.2012.09.004.
35. GitHub. Available at: https://github.com/SevalTorunYeter/WMH_detecting_with_Masks [Accessed: 22.04.2024]
36. Grimaud J, Lai M, Thorpe J, Adeleine P, Wang L, Barker GJ, et al. Quantification of MRI lesion load in multiple sclerosis: A comparison of three computer-assisted techniques. Magn Reson Imaging 1996;14:495-505. doi: 10.1016/0730-725x(96)00018-5.
37. Payne ME, Fetzer DL, MacFall JR, Provenzale JM, Byrum CE, Krishnan KR. Development of a semi-automated method for quantification of MRI gray and white matter lesions in geriatric subjects. Psychiatry Res 2002;115:63-77. doi: 10.1016/s0925-4927(02)00009-4.
38. Valverde S, Oliver A, Roura E, Pareto D, Vilanova JC, Ramió-Torrentà L, et al. Quantifying brain tissue volume in multiple sclerosis with automated lesion segmentation and filling. Neuroimage Clin 2015;9:640-7. doi: 10.1016/j.nicl.2015.10.012.
39. Bartko JJ. Measurement and reliability: Statistical thinking considerations. Schizophr Bull 1991;17:483-9. doi: 10.1093/schbul/17.3.483.